

## Improved Understanding of Stent Malapposition Using Virtual Bench Testing

Peter Mortier,<sup>1,2</sup> Heleen MM van Beusekom,<sup>3</sup> Matthieu De Beule,<sup>1,2</sup> Ilona Krabbendam-Peters,<sup>3</sup> Benjamin Van Der Smissen,<sup>2,4</sup> Gianluca De Santis,<sup>2</sup> Jurgen M Ligthart,<sup>3</sup> Benedict Verhegghe<sup>1,2</sup> and Wim J van der Giessen†<sup>3,5</sup>

1. FEops bvba, Ghent; 2. IBiTech-bioMMeda, Ghent University; 3. Thoraxcenter, Erasmus Medical Center, Rotterdam;

4. University College Ghent, Department of Mechanics, Ghent; 5. ICIN-KNAW, Utrecht

### Abstract

Intravascular imaging techniques such as optical coherence tomography (OCT) and intravascular ultrasound (IVUS) are often used to assess strut apposition, but only provide limited insight into the three-dimensional appositioning behaviour of stents. Recently, a new approach has been introduced to study the phenomenon of incomplete stent apposition (ISA) based on finite element simulations. In this study, we employed this virtual strut apposition assessment technique in the setting of coronary bifurcation stenting and compared simulated strut–artery distances of two stent designs with actual measurements based on OCT imaging using a silicone model. Stenting of the main branch leads to malapposed struts in the proximal part and the average strut–artery distance in that region for the Integrity stent is 126  $\mu\text{m}$  based on the simulation and 117 $\pm$ 14  $\mu\text{m}$  based on the OCT analysis. For the Multi-Link 8 stent, this average distance is 150  $\mu\text{m}$  and 174 $\pm$ 7  $\mu\text{m}$  for the simulation and the *in vitro* OCT measurements respectively. In conclusion, the virtual assessment of strut appositioning results in similar strut–artery distances when compared with measurements based on OCT-visualised *in vitro* stent deployments and could be used to optimise devices and procedures.

### Keywords

Stent strut apposition, finite element simulations, bench testing, optical coherence tomography

**Disclosure:** Medtronic provided a research grant for this study and has delivered all stent and balloon samples. Peter Mortier, Matthieu De Beule and Benedict Verhegghe are shareholders of FEops, an engineering consultancy spin-off from Ghent University, and have served as consultants for several medical device companies.

**Dedicated to:** This work is dedicated to Wim J van der Giessen†, deceased.

**Acknowledgements:** The authors acknowledge Medtronic for providing a research grant for this study and for delivering all stent and balloon samples, Francesco Iannaccone for his valuable assistance to optimise the post-processing of the simulation data, Dassault Systèmes SIMULIA BV for the software licence and Karin Witberg for assistance during acquisition of the OCT images.

**Received:** 20 July 2011 **Accepted:** 8 August 2011 **Citation:** *Interventional Cardiology*, 2011;6(2):106–9

**Correspondence:** Peter Mortier, IIC UGent, Technologiepark 3/13, 9052 Ghent, Belgium. E: peter.mortier@feops.com

Incomplete stent apposition (ISA) or stent malapposition is the lack of contact between stent struts and the underlying arterial wall. ISA has been associated with significantly higher levels of thrombus deposition<sup>1</sup> and is typically assessed by intravascular imaging techniques such as optical coherence tomography (OCT) and intravascular ultrasound (IVUS).<sup>2–4</sup> These imaging modalities are useful to see whether or not malapposition occurs, albeit within the limit of detection of these modalities, but the resulting cross-sectional images do not allow a detailed analysis of the overall appositioning behaviour of the stent. For example, from these 2D images it is hard to investigate whether or not certain parts of a stent design are more vulnerable to malapposition. Recently, we have introduced a new approach to study the phenomenon of ISA based on finite element simulations.<sup>5</sup> Such simulations are used during the development process of new devices as they allow the optimisation of a design without having to manufacture every intermediate design iteration. They have also proven to be a valuable tool to investigate and optimise interventional procedures such as bifurcation stenting.<sup>6–7</sup> Standard results from these simulations are the stent and vessel deformations and the internal stresses and strains. Based on the predicted deformations, the strut–artery distance can be calculated over the complete stent length, giving additional insights into the 3D appositioning behaviour.

In this paper, we applied this virtual strut apposition assessment technique in the setting of bifurcation stenting, associated with a high degree of malapposition in certain cases. The strut–artery distances predicted by the simulations were compared with measurements based on OCT imaging following *in vitro* stent deployment.

### Materials and Methods

#### Bifurcation Model

Commercially available stents were deployed in a stenotic bifurcation model using a provisional approach. This was achieved virtually using finite element simulations and *in vitro* using silicone models, allowing for a comparison of the strut malapposition measured with both approaches. The diameters of the proximal main vessel, the distal main vessel and the side branch are 3.5 mm, 2.8 mm and 2.5 mm respectively, leading to a model in agreement with Finet's and Murray's law.<sup>8–9</sup> The silicone models were built using rapid prototyping techniques (Objet Eden 350V printer, Objet Geometries Inc., Billerica, MA).

#### Stents

The stents used for this study were the bare metal Integrity stent (Medtronic, Minneapolis, MN) and Multi-Link 8 stent (Abbott Vascular, Santa Clara, CA). Stent sizes (3.0 mm x 18 mm) were taken according

to the distal main vessel, following the recommendation of the European Bifurcation Club.<sup>10</sup>

### Stent Deployment and Postdilatation

Stents were placed over the side branch. Initial deployment pressure was chosen to achieve a balloon:artery ratio of 1.1:1 in the distal main branch. Effectively, 9 atm was used for the Integrity stent and 11 atm for the Multi-Link 8 stent. Postdilatation of the segment proximal to the side branch was performed using a 3.5 mm balloon that was inflated at 15 atm in the proximal main vessel to reach a balloon–artery ratio of 1.1:1 at the proximal segment. This proximal optimisation technique (POT) improves the strut apposition in the proximal main vessel and is recommended in case of difficulty re-crossing into the side branch.<sup>11</sup> Final kissing inflation was not performed. The employed stenting procedure is depicted in *Figure 1*, as well as the virtual and silicone bifurcation model.

### In Vitro Optical Coherence Tomography Imaging

Two samples of each stent were deployed at room temperature in the silicone models described above. The silicone models were submerged in a Ringer's lactate solution during the complete stenting procedure. OCT (C7 Dragonfly™, St Jude Medical, St Paul, MN) was performed before and after stent deployment and after postdilating the proximal main vessel with a pullback speed of 10 mm/s. The resulting images were quantitatively analysed using dedicated software (QCU-CMS, Medis Medical Imaging Systems, Leiden, The Netherlands). In particular, stent malapposition in the non-diseased proximal main vessel after initial stent deployment was quantified by averaging the individual strut–artery distances in five OCT images. OCT only accurately shows the endoluminal strut surface and, therefore, strut thickness (93 µm for the Integrity stent, 81 µm for the Multi-Link 8 stent) was subtracted from the measured values. In addition, the stent area was determined at the location of maximal narrowing.

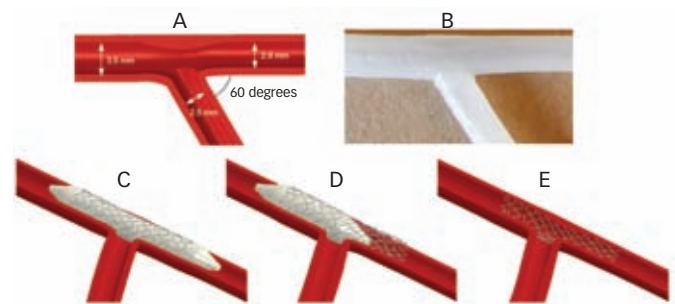
### Finite Element Simulations

Stent models were generated starting from high-resolution micro-computed tomography (CT) images of the crimped stents<sup>5</sup> and material properties were taken from O'Brien et al.<sup>12</sup> Then the stents were combined with folded balloon models that led to a realistic compliance behaviour of the balloon-stent systems. This was verified by comparing the virtual compliance behaviour with the data reported by the stent manufacturers, showing that the maximum percentage difference in diameter was less than 1 % within the applied pressure range. The same accuracy in compliance behaviour was obtained for the post-dilatation balloon model. The virtual stenting procedure was performed using the Abaqus/Explicit finite element solver (Dassault Systèmes SIMULIA, Providence, RI). The virtually stented artery models were then imported in pyFormex (www.pyFormex.org) where the strut apposition measurements were performed, both after initial stent deployment and after post-dilatation. The procedure allows automated quantification of the strut–artery distance in every node lying on the (outer) strut surface. For the calculation of the average strut–artery distance in the non-diseased part of the proximal main vessel, only the values in the nodes from the centreline of the outer stent surface were considered. For the Integrity stent, which has circular struts, the initial outermost point of the struts was considered.

### Results

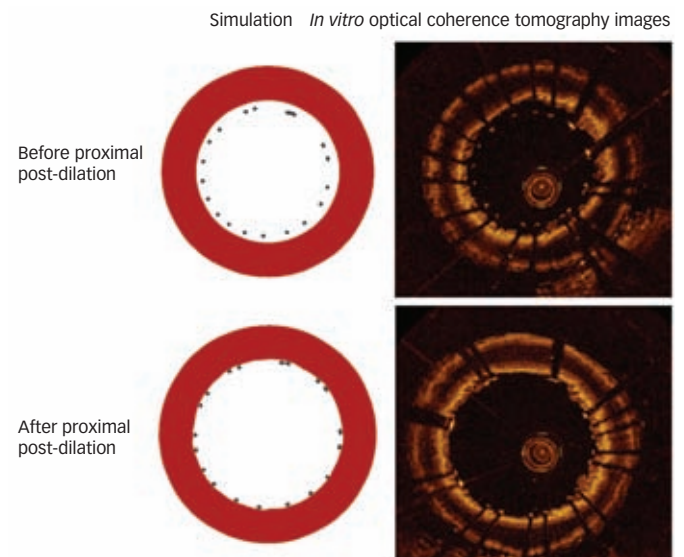
Stent sizing according to the distal main vessel typically leads to malapposition in the proximal main vessel, which can be optimised by a

**Figure 1: Illustration of the Bifurcation Model and the Stenting Procedure**



A 3D stenotic computer model of a coronary bifurcation was created with a bifurcation angle of 60 degrees. The branch diameters were chosen in agreement with Finet's and Murray's branching laws (A). Silicone representations of this bifurcation model were then generated using rapid prototyping techniques (B) and used for in vitro bench deployments. Similarly, virtual bench testing was performed using the original virtual bifurcation model. The same stenting procedure was performed in both cases: stent deployment in the main vessel (C) followed by post-dilatation of the proximal main vessel (D). The final configuration is depicted in panel E.

**Figure 2: Comparison of Strut Apposition Before (Top) and After Proximal Post-dilatation (Bottom)**

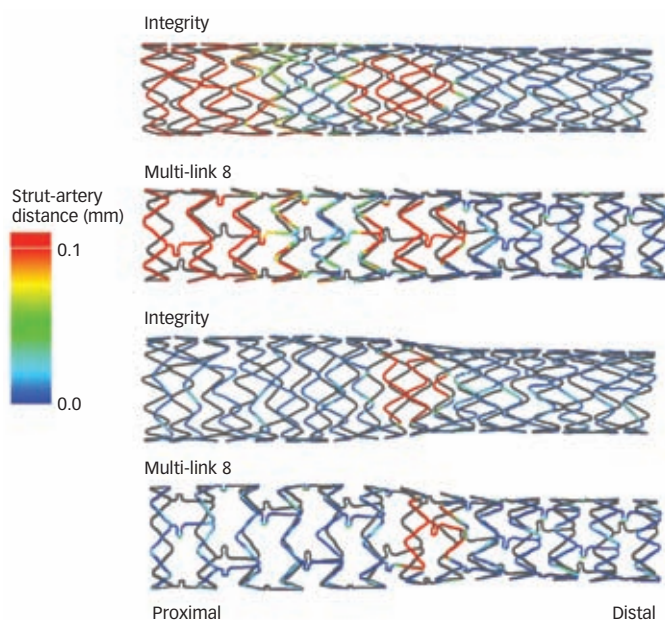


Post-dilating the proximal main vessel leads to a good apposition of the floating struts, as shown by the simulation results (left) and the optical coherence tomography images (right).

proximal post-dilatation as shown in *Figure 2*. Based on the simulation results, the post-dilatation reduces the average strut–artery distance in the healthy proximal main vessel from 126 µm to 4 µm for the Integrity stent, and from 150 µm to 10 µm for the Multi-Link 8 stent.

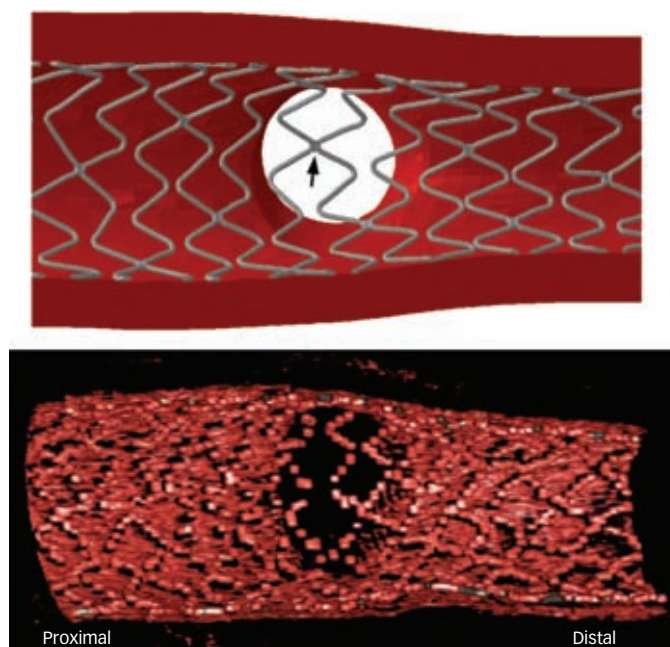
The contour plots shown in *Figure 3* are based on the simulations and illustrate the stent strut apposition of the different investigated stents before and after post-dilatation. A blue colour corresponds with a minimal distance between the struts and the inner arterial wall and thus with a good apposition of the stent struts, whereas a red colour reflects a larger strut–artery distance. This figure illustrates again the impact of the post-dilatation on strut apposition in the proximal stent segment. The red coloured region in the centre of the stent corresponds with the floating struts at the side branch ostium. The impact of post-dilatation can also be assessed by quantifying the percentage of struts at a distance larger than 20 µm. Post-dilatation reduces this percentage from 47 % to 8 % for the Integrity stent, and from 54 % to 16 % for the Multi-Link 8 stent.

**Figure 3: Contour Plot of Strut Apposition of the Two Stents Before (Top) and After Post-dilation (Bottom)**



The colours reflect the distance between the strut surface and the inner surface of the arterial wall (blue colour = well apposed, red colour = malapposed). Malapposition can be observed in the proximal stent region before post-dilation and in the centre of the stent, where floating struts are present at the side branch ostium.

**Figure 4: Illustration of the Postdilated Integrity Stent Overlying the Side Branch Ostium**



In the simulated case (top), there is a connection between the struts located at the side branch ostium (arrow) that limits the expansion of the struts into the side branch. The bottom panel shows a 3D OCT reconstruction.

The comparison of the simulation results and the OCT measurements is summarised in Table 1. For the Integrity stent, the simulation predicts an average malapposition (in the proximal main vessel) of 126  $\mu\text{m}$ , while the analysis of the OCT images resulted in an average strut–artery distance of  $117 \pm 14 \mu\text{m}$ . For the Multi-Link 8 stent, this average distance is 150  $\mu\text{m}$  and  $174 \pm 7 \mu\text{m}$  for the simulation and the *in vitro* OCT measurements, respectively. In

**Table 1: Quantitative Comparison of Simulation Results and the Optical Coherence Tomography Measurements in Terms of Strut–Artery Distance and Stent Area at the Location of Maximal Stenosis**

	After Stenting		After Post-dilation	
	Simulation	OCT	Simulation	OCT
<b>Strut–artery distance</b>				
Integrity	126 $\mu\text{m}$	$117 \pm 14 \mu\text{m}$	4 $\mu\text{m}$	-
Multi-Link 8	150 $\mu\text{m}$	$174 \pm 7 \mu\text{m}$	10 $\mu\text{m}$	-
<b>Stent area</b>				
Integrity	6.59 $\text{mm}^2$	$6.64 \pm 0.18 \text{mm}^2$	8.70 $\text{mm}^2$	$9.94 \pm 0.23 \text{mm}^2$
Multi-Link 8	6.53 $\text{mm}^2$	$6.33 \pm 0.23 \text{mm}^2$	8.56 $\text{mm}^2$	$8.81 \pm 1.76 \text{mm}^2$

Strut–artery distance is not reported after post-dilation for the optical coherence tomography measurements as the resolution of the images does not allow accurate analysis of very small distances. OCT = optical coherence tomography.

addition, Table 1 also contains the stent area at the location of maximal stenosis before and after post-dilation, based on both the simulations and the OCT analysis.

### Discussion

Stent malapposition is typically investigated by intravascular imaging modalities such as IVUS and OCT, the latter having a higher resolution (15  $\mu\text{m}$  versus 150  $\mu\text{m}$ ), which may reveal malapposition in greater detail. Recently, a new approach has been introduced to study the phenomenon of ISA, based on finite element simulations.<sup>5</sup> In the present study, both approaches were compared when stenting the main branch of a bifurcation using the same stenting procedure and bifurcation model during an *in vitro* and virtual bench test, and the obtained strut apposition results corresponded well. The small differences can be attributed to many factors, such as assumptions made for the finite element modelling, inaccuracies in the silicone models, limited resolution of the OCT images and small procedural differences (e.g. applied pressure).

The virtual strut apposition assessment may help to better understand and to minimise acute ISA as it gives additional information compared with traditional evaluation methods (IVUS and OCT). A first advantage is that the strut–artery distance can be quantified and visualised over the complete stent length, while currently used ISA measurements are typically based on IVUS and OCT cross-sectional images. This allows identification of the location of the malapposed struts with respect to the artery and plaque morphology. Furthermore, the impact of different stent designs can be investigated and the apposition behaviour of new stents could be optimised during the design phase. The detailed contour plots shown in Figure 3 reveal, for example, the occurrence of a small gap at the location of every U-turn in the bridging members of the Multi-Link 8 design. This gap seems to be caused by the strong circumferential curvature of this U-turn. The proposed virtual ISA measurement procedure could also be used to investigate and quantify the impact of different post-dilation strategies (e.g., balloon compliance, balloon pressure) and could provide additional insight in more complex bifurcation stenting techniques, where large strut malapposition frequently occurs.

Both the OCT measurement and the simulation results indicate that the Integrity stent struts are slightly closer to the vessel wall as compared with the Multi-Link 8 stent, both before and after

post-dilation. The difference in strut thickness between the two stents partially explains this finding, but other factors are affecting this strut–artery distance, such as the expanded stent diameter at maximal balloon pressure, strut shape and stent recoil.

The *in vitro* and virtual deployments have been further compared by quantifying the stent area at the location of maximal stenosis. The obtained stent areas correspond well before post-dilation, but a considerable difference (1.24 mm<sup>2</sup>) can be observed after post-dilation of the Integrity stent. A different rotational position of the stent during the *in vitro* and virtual bench test could explain this discrepancy. There is, for example, a connection or weld between the struts located at the side branch ostium during the simulated case that limits the expansion of the struts into the side branch and thus the measured stent area (Figure 4).

The virtual stent apposition analysis has up to now only been used for research purposes, using simplified arterial models. It would of course be valuable to obtain this kind of highly detailed strut apposition measurement when treating real patients and there might be two alternative approaches to reach this goal: a first one could be based on

advanced OCT image analysis and reconstruction. It should be feasible to create similar 3D contour plots of ISA over the complete stent length using 3D OCT reconstructions (see Figure 4). Such analysis would require robust and automatic strut and lumen detection methods. Alternatively, simulations based on pre-operative patient images (e.g. CT combined with IVUS<sup>13</sup> or OCT to gain a higher resolution) could be used to study strut apposition using the same methodology as presented in this study. This approach, which is at least as ambitious as the first one, would allow very detailed strut apposition analysis (see Figure 3), but the predictive power of these simulations for real patient treatment first needs to be proven.

## Conclusion

The assessment of strut apposition using computer simulations results in similar strut–artery distances when compared with measurements based on OCT-visualised *in vitro* stent deployments. Furthermore, it allows detailed three-dimensional visualisation of strut–artery distances over the complete stent length, providing useful insights into the phenomenon of stent strut malapposition. This approach could be applied to optimise devices and procedures. ■

- Ozaki Y, Okumura M, Ismail TF, et al., The fate of incomplete stent apposition with drug-eluting stents: an optical coherence tomography-based natural history study, *Eur Heart J*, 2010;31:1470–6.
- Hassan AKM, Bergheanu SC, Stijnen T, et al., Late stent malapposition risk is higher after drug-eluting stent compared with bare-metal stent implantation and associates with late stent thrombosis, *Eur Heart J*, 2010;31:1172–80.
- Cook S, Wenaweser P, Togni M, et al., Incomplete stent apposition and very late stent thrombosis after drug-eluting stent implantation, *Circulation*, 2007;115:2426–34.
- Radu M, Jorgensen E, Kelbaek H, et al., Strut apposition after coronary stent implantation visualised with optical coherence tomography, *EuroIntervention*, 2010;6:86–93.
- Mortier P, De Beule M, Segers P, et al., Virtual bench testing of new generation coronary stents, *EuroIntervention*, accepted for publication.
- Mortier P, Holzapfel GA, De Beule M, et al., A novel simulation strategy for stent insertion and deployment in curved coronary bifurcations: comparison of three drug-eluting stents, *Ann Biomed Eng*, 2010;38:88–99.
- Mortier P, Computer modelling of coronary bifurcation stenting, PhD Thesis, Ghent University, Belgium, 2010.
- Murray CD, The physiological principle of minimum work. I. The vascular system and the cost of blood volume, *Proc Natl Acad Sci USA*, 1926;12:207–14.
- Finet G, Gilard M, Perrenot B, et al., Fractal geometry of arterial coronary bifurcations: a quantitative coronary angiography and intravascular ultrasound analysis, *EuroIntervention*, 2007;3:490–8.
- Stankovic G, Darremont O, Ferenc M, et al., Percutaneous coronary intervention for bifurcation lesions: 2008 consensus document from the fourth meeting of the European Bifurcation Club, *EuroIntervention*, 2009;5:39–49.
- Hildick-Smith D, Lassen JF, Albiero R, et al., Consensus from the 5th European Bifurcation Club meeting, *EuroIntervention*, 2010;6:34–8.
- O'Brien BJ, Stinson JS, Larsen SR, et al., A platinum–chromium steel for cardiovascular stents, *Biomaterials*, 2010;31:3755–61.
- van der Giessen A, Schaap M, Gijzen F, et al., 3D fusion of intravascular ultrasound and coronary computed tomography for in-vivo wall shear stress analysis – a feasibility study, *Int J Cardiovasc Imaging*, 2010;26:781–96.